The International Journal of Advanced Manufacturing Technology (2022) 120:8105–8115
https://doi.org/10.1007/s00170-022-09245-6

ORIGINAL ARTICLE

An improved numerical integration method for prediction of milling stability using the Lagrange-Simpson interpolation scheme

Yan Xia[1] · Yi Wan[2] · Guosheng Su[1] · Jin Du[1] · Peirong Zhang[1] · Chonghai Xu[1]

Received: 14 December 2021 / Accepted: 18 April 2022 / Published online: 7 May 2022

Abstract

The stability prediction is usually used to avoid the unstable machining in milling process. According to the Lagrange-Simpson hybrid interpolation scheme, this paper improves a numerical integration method (NIM) to perform the milling chatter prediction accurately and efficiently. Firstly, the higher-order numerical integral formulas (NIFs) are constructed based on the Lagrange polynomial. Thus, the third-order and fourth-order NIMs are built and investigated respectively. Then, to improve the calculated performance of the NIMs, the Simpson scheme is introduced to decrease the local discretization error. Finally, the comparisons among the built NIMs and the existing discretization methods are carried out by calculating the convergence rate and the stability boundaries. Compared to the third-order NIM and the third-order full-discretization method, the proposed second-order Lagrange-Simpson NIM shows the better computational performance.

Keywords Milling stability prediction · Numerical integration method · Polynomial interpolation · Simpson rule · Local discretization error

1 Introduction

During machining process, chatter vibration easily leads to several negative effects, such as the poor machined quality, defective accuracy, harsh noise, and even tool damage [1]. An effective method to avoid the chatter is to carry out the stability boundaries prediction of the machining system, which can guide the proper selection of the cutting parameters [2]. Up to now, many approaches are proposed to achieve the chatter stability prediction, mainly including the analytical method, the numerical method, and the experimental method [3].

Based on the Fourier series of the system coefficients, Altintas and Budak developed the zeroth-order approximation (ZOA) method [4]. In order to improve the applicability of the method, the multi-frequency method was investigated and extended [5, 6]. Then, these analytical methods were used to predict the stability zones of the non-standard cutting tools or the thin-walled parts [7, 8].

Unlike the analytical method, the numerical method focuses on how to accurately and efficiently estimate the delay differential equation described the dynamic machining process [9]. The semi-discretization method (SDM), the full-discretization method (FDM), and the numerical integration method (NIM) were explored and improved successively. To achieve the stability prediction, Insperger and Stépán early proposed the zeroth-order SDM, and then expanded the SDM with the higher order [10–12]. Likewise, Zhan et al. built the second-order SDM to accurately obtain the stability prediction [13]. To overcome the low efficiency of the SDM, Ding et al. developed the FDM, and the computational results demonstrated that the method has high efficiency. Subsequently, the FDMs were improved using the Lagrange polynomial, Newton polynomial, or Hermite polynomial. For instance, the second-order FDMs were constructed, where the state item of the system was estimated using the second-order Lagrange polynomial [14, 15]. Similarly, the third-order Newton or Hermite polynomial was used to build the third-order FDM [16–21]. When the order of the interpolation polynomial increases, the computational accuracy of the corresponding FDM is

✉ Yan Xia
yxia@qlu.edu.cn

[1] School of Mechanical Engineering, Qilu University of Technology (Shandong Academy of Sciences), Jinan 250353, China

[2] Key Laboratory of High Efficiency and Clean Mechanical Manufacture, Ministry of Education, School of Mechanical Engineering, Shandong University, Jinan 250061, China

improved, whereas the computational cost increases obviously as well.

In order to further improve the prediction performance, Ding et al. used the Newton–Cotes formulas to construct the NIM, where the calculated results verified the high efficiency and high accuracy of the method [22]. Then, according to the Simpson formula, Zhang et al. proposed a novel NIM, where the corresponding convergence rate was higher than those of some existing discretization methods [23]. Subsequently, Ozoegwu built the higher-order NIMs by using the higher vector numerical integration schemes [24]. Furthermore, several numerical methods based on the Adams relative formulas were built respectively, such as the Adams–Moulton method [25], the implicit Adams method [26], and the Adams–Bashforth method [27]. Likewise, the Chebyshev-based methods were investigated to perform the accurate and efficient stability prediction [28–30].

Based on the second-order Lagrange polynomial, Xia et al. proposed the improved NIM, in which the method was more accurate compared with the first-order NIM [31]. In reference [31], the first two-order NIFs were derived using the Lagrange integral scheme to build the second-order NIM. However, the higher-order NIFs are not introduced, and the local discretization error is limited due to the used trapezoidal rule. Therefore, this paper studies the effect of the higher-order NIFs on the computational performance; on the basis, the Simpson scheme is introduced to improve the NIM for decreasing the local discretization error.

The paper is organized as follows. Section 2 derives the algorithm of the third-order and fourth-order NIMs. Then, the effect of the interpolation order on the chatter stability prediction is analyzed in Sect. 3. In Sect. 4, the Simpson scheme is introduced to improve the NIMs. Finally, Sect. 5 presents some brief conclusions.

2 Algorithm of the higher-order numerical integration methods

The regenerative milling dynamics can be described by the form of state space equation [14, 31]:

$$\dot{\mathbf{x}}(t) = \mathbf{A}_0\mathbf{x}(t) + \mathbf{A}(t)[\mathbf{x}(t) - \mathbf{x}(t-T)] \tag{1}$$

where the matrixes $\mathbf{A}_0$ and $\mathbf{A}$ present the natural and dynamic traits of the machining system respectively, which can be described as:

$$\mathbf{A}_0 = \begin{bmatrix} -\mathbf{M}^{-1}\mathbf{C}/2 & \mathbf{M}^{-1} \\ \mathbf{C}\mathbf{M}^{-1}\mathbf{C}/4 - \mathbf{K} & -\mathbf{C}\mathbf{M}^{-1}/2 \end{bmatrix} \quad \mathbf{A}(t) = \begin{bmatrix} 0 \\ a_p\mathbf{K}_c(t) \end{bmatrix} \tag{2}$$

Based on the direct integration method [3], the solution of Eq. (1) is expressed as:

$$\mathbf{x}(t) = e^{\mathbf{A}_0(t-t_0)}\mathbf{x}(t_0) + \int_{t_0}^{t} \left\{ e^{\mathbf{A}_0(t-\xi)}\mathbf{A}(\xi)[\mathbf{x}(\xi) - \mathbf{x}(\xi - T)] \right\} d\xi \tag{3}$$

To solve the Eq. (3), the first two-order NIMs were proposed according to the Lagrange integral scheme in reference [31]. Then, the third-order and fourth-order NIMs will be constructed in this paper. According to the integral scheme in the reference [31], the third-order and fourth-order NIFs are built respectively, which can be written as:

$$\int_{x_i}^{x_{i+1}} f(x)\,dx \approx \frac{h}{24}\left[9f(x_i) + 19f(x_{i+1}) - 5f(x_{i+2}) + f(x_{i+3})\right] \tag{4}$$

$$\int_{x_i}^{x_{i+1}} f(x)\,dx \approx \frac{h}{720}\begin{bmatrix} 251f(x_i) + 646f(x_{i+1}) - 264f(x_{i+2}) \\ +106f(x_{i+3}) - 19f(x_{i+4}) \end{bmatrix} \tag{5}$$

where x_j ($j = i, i+1, i+2, i+3$, and $i+4$) denotes the discrete points, and $h = x_{i+1}\text{-}x_i$ stands for the discrete interval.

2.1 Third-order numerical integration method (3rd NIM)

As shown in Fig. 1, a whole tooth passing period (T) in milling operation includes the free vibration interval (T_f) and forced vibration interval (T_u). The time points t_0 and t_1 are the endpoints of the free vibration interval. Thus, based on the Eq. (3), at time point t_1, $\mathbf{x}(t_1)$ becomes:

$$\mathbf{x}(t_1) = e^{\mathbf{A}_0 T_f}\mathbf{x}(t_0) \tag{6}$$

According to the Eq. (4), $\mathbf{x}(t_2)$ at time point t_2 is described by:

$$\mathbf{x}(t_2) = e^{\mathbf{A}_0(t_2-t_1)}\mathbf{x}(t_1) + \frac{\tau}{24}\begin{Bmatrix} 9e^{\mathbf{A}_0(t_2-t_1)}\mathbf{A}(t_1)[\mathbf{x}(t_1) - \mathbf{x}(t_1 - T)] + \\ 19\mathbf{A}(t_2)[\mathbf{x}(t_2) - \mathbf{x}(t_2 - T)] - \\ 5e^{\mathbf{A}_0(t_2-t_3)}\mathbf{A}(t_3)[\mathbf{x}(t_3) - \mathbf{x}(t_3 - T)] + \\ e^{\mathbf{A}_0(t_2-t_4)}\mathbf{A}(t_4)[\mathbf{x}(t_4) - \mathbf{x}(t_4 - T)] \end{Bmatrix} \tag{7}$$

When $t = t_i$ ($i = 3, 4, \ldots, m-1$), where m is the discretization number, the value $\mathbf{x}(t_i)$ can be expressed by:

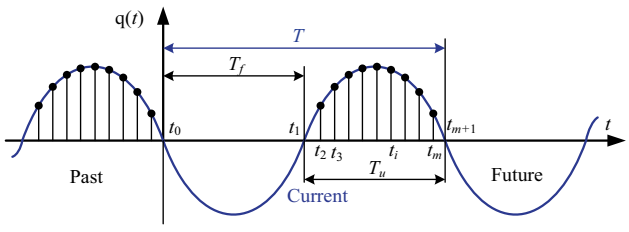

Fig. 1 The discrete scheme of the milling process [31]

$$\mathbf{x}(t_i)=e^{\mathbf{A}_0(t_i-t_{i-1})}\mathbf{x}(t_{i-1})+\frac{\tau}{24}\begin{Bmatrix}9e^{\mathbf{A}_0(t_i-t_{i-1})}\mathbf{A}(t_{i-1})[\mathbf{x}(t_{i-1})-\mathbf{x}(t_{i-1}-T)]+\\19\mathbf{A}(t_i)[\mathbf{x}(t_i)-\mathbf{x}(t_i-T)]-\\5e^{\mathbf{A}_0(t_i-t_{i+1})}\mathbf{A}(t_{i+1})[\mathbf{x}(t_{i+1})-\mathbf{x}(t_{i+1}-T)]+\\e^{\mathbf{A}_0(t_i-t_{i+2})}\mathbf{A}(t_{i+2})[\mathbf{x}(t_{i+2})-\mathbf{x}(t_{i+2}-T)]\end{Bmatrix} \tag{8}$$

The values $\mathbf{x}(t_i)$ at $t=t_m$ and t_{m+1} cannot be described by Eq. (8), since $\mathbf{x}(t_{m+2})$ and $\mathbf{x}(t_{m+3})$ do not exist. For time point t_i ($i=m$ or $m+1$), $\mathbf{x}(t_i)$ should be approximated according to the trapezoidal rule:

$$\mathbf{x}(t_i)=e^{\mathbf{A}_0(t_i-t_{i-1})}\mathbf{x}(t_{i-1})+\frac{\tau}{2}\begin{Bmatrix}e^{\mathbf{A}_0(t_i-t_{i-1})}\mathbf{A}(t_{i-1})[\mathbf{x}(t_{i-1})-\mathbf{x}(t_{i-1}-T)]+\\\mathbf{A}(t_i)[\mathbf{x}(t_i)-\mathbf{x}(t_i-T)]\end{Bmatrix} \tag{9}$$

Substituting Eqs. (6)–(9) into Eq. (3), resulting in the discrete map as follows:

$$(\mathbf{I}-\mathbf{D}_3-\frac{\tau}{24}\mathbf{E}_3)\begin{bmatrix}\mathbf{x}(t_1)\\\mathbf{x}(t_2)\\\vdots\\\mathbf{x}(t_{m+1})\end{bmatrix}=(\mathbf{F}_3-\frac{\tau}{24}\mathbf{E}_3)\begin{bmatrix}\mathbf{x}(t_1-T)\\\mathbf{x}(t_2-T)\\\vdots\\\mathbf{x}(t_{m+1}-T)\end{bmatrix} \tag{10}$$

where

$$\mathbf{D}_3=\begin{bmatrix}0&&&&\\e^{\mathbf{A}_0\tau}&0&&&\\&e^{\mathbf{A}_0\tau}&0&&\\&&\ddots&\ddots&\\&&&e^{\mathbf{A}_0\tau}&0\end{bmatrix}\quad\mathbf{F}_3=\begin{bmatrix}0&\cdots&0&e^{\mathbf{A}_0T_f}\\0&0&0&0\\&\ddots&&\\&&0&\\0&&&0\end{bmatrix}$$

$$\mathbf{E}_3=\begin{bmatrix}0&&&&&\\9e^{\mathbf{A}_0\tau}\mathbf{A}_1&19\mathbf{A}_2&-5e^{-\mathbf{A}_0\tau}\mathbf{A}_3&e^{-2\mathbf{A}_0\tau}\mathbf{A}_4&&\\&\ddots&\ddots&\ddots&\ddots&\\&&9e^{\mathbf{A}_0\tau}\mathbf{A}_{m-2}&19\mathbf{A}_{m-1}&-5e^{-\mathbf{A}_0\tau}\mathbf{A}_m&e^{-2\mathbf{A}_0\tau}\mathbf{A}_{m+1}\\&&&12e^{\mathbf{A}_0\tau}\mathbf{A}_{m-1}&12\mathbf{A}_m&\\&&&&12e^{\mathbf{A}_0\tau}\mathbf{A}_m&12\mathbf{A}_{m+1}\end{bmatrix} \tag{11}$$

Here, $\mathbf{A}_i$ denotes $\mathbf{A}(t_i)$ ($i=1, 2, 3\ldots$).

For the milling system, its transition matrix $\boldsymbol{\Phi}$ on the period T is derived as:

$$\boldsymbol{\Phi}=(\mathbf{I}-\mathbf{D}_3-\frac{\tau}{24}\mathbf{E}_3)^{-1}(\mathbf{F}_3-\frac{\tau}{24}\mathbf{E}_3) \tag{12}$$

Then, the stability boundaries can be predicted based on the Floquet theory.

2.2 Fourth-order numerical integration method (4th NIM)

According to the Eq. (5), $\mathbf{x}(t_2)$ at time point t_2 is expressed by:

$$\mathbf{x}(t_2)=e^{\mathbf{A}_0(t_2-t_1)}\mathbf{x}(t_1)+\frac{\tau}{720}\begin{Bmatrix}251e^{\mathbf{A}_0(t_2-t_1)}\mathbf{A}(t_1)[\mathbf{x}(t_1)-\mathbf{x}(t_1-T)]+\\646\mathbf{A}(t_2)[\mathbf{x}(t_2)-\mathbf{x}(t_2-T)]-\\264e^{\mathbf{A}_0(t_2-t_3)}\mathbf{A}(t_3)[\mathbf{x}(t_3)-\mathbf{x}(t_3-T)]+\\106e^{\mathbf{A}_0(t_2-t_4)}\mathbf{A}(t_4)[\mathbf{x}(t_4)-\mathbf{x}(t_4-T)]-\\19e^{\mathbf{A}_0(t_2-t_5)}\mathbf{A}(t_5)[\mathbf{x}(t_5)-\mathbf{x}(t_5-T)]+\end{Bmatrix} \tag{13}$$

Likewise, at time point $t=t_i$ ($i=3,4,\ldots,m$-2),the relevant response $\mathbf{x}(t_i$

$$\mathbf{x}(t_i)=e^{\mathbf{A}_0(t_i-t_{i-1})}\mathbf{x}(t_{i-1})+\frac{\tau}{720}\begin{Bmatrix}251e^{\mathbf{A}_0(t_i-t_{i-1})}\mathbf{A}(t_{i-1})[\mathbf{x}(t_{i-1})-\mathbf{x}(t_{i-1}-T)]+\\646\mathbf{A}(t_i)[\mathbf{x}(t_i)-\mathbf{x}(t_i-T)]-\\264e^{\mathbf{A}_0(t_i-t_{i+1})}\mathbf{A}(t_{i+1})[\mathbf{x}(t_{i+1})-\mathbf{x}(t_{i+1}-T)]+\\106e^{\mathbf{A}_0(t_i-t_{i+2})}\mathbf{A}(t_{i+2})[\mathbf{x}(t_{i+2})-\mathbf{x}(t_{i+2}-T)]-\\19e^{\mathbf{A}_0(t_i-t_{i+3})}\mathbf{A}(t_{i+3})[\mathbf{x}(t_{i+3})-\mathbf{x}(t_{i+3}-T)]+\end{Bmatrix} \tag{14}$$

However, at time point $t=t_i$ ($i=m-1$, m, or $m+1$), Eq. (14) is not unfit to $\mathbf{x}(t_i)$. This is because of the inexistence of $\mathbf{x}(t_i)$ ($i=m-1$, m, or $m+1$). Thereby, the trapezoidal rule is used to express the value of $\mathbf{x}(t_i)$ at t_i ($i=m-1$, m, or $m+1$), which can be written as:

$$\mathbf{x}(t_i)=e^{\mathbf{A}_0(t_i-t_{i-1})}\mathbf{x}(t_{i-1})+\frac{\tau}{2}\begin{Bmatrix}e^{\mathbf{A}_0(t_i-t_{i-1})}\mathbf{A}(t_{i-1})[\mathbf{x}(t_{i-1})-\mathbf{x}(t_{i-1}-T)]+\\\mathbf{A}(t_i)[\mathbf{x}(t_i)-\mathbf{x}(t_i-T)]\end{Bmatrix} \tag{15}$$

Combining Eqs. (6), (13)–(15) to express Eq. (3), the discrete map is derived as follows:

$$(\mathbf{I}-\mathbf{D}_4-\frac{\tau}{720}\mathbf{E}_4)\begin{bmatrix}\mathbf{x}(t_1)\\\mathbf{x}(t_2)\\\vdots\\\mathbf{x}(t_{m+1})\end{bmatrix}=(\mathbf{F}_4-\frac{\tau}{720}\mathbf{E}_4)\begin{bmatrix}\mathbf{x}(t_1-T)\\\mathbf{x}(t_2-T)\\\vdots\\\mathbf{x}(t_{m+1}-T)\end{bmatrix} \tag{16}$$

Here, matrix $\mathbf{E}_4$ is listed in Appendix, matrixes $\mathbf{D}_4$ and $\mathbf{F}_4$ are represented by:

$$\mathbf{D}_4=\begin{bmatrix}0&&&&\\e^{\mathbf{A}_0\tau}&0&&&\\&e^{\mathbf{A}_0\tau}&0&&\\&&\ddots&\ddots&\\&&&e^{\mathbf{A}_0\tau}&0\end{bmatrix}\quad\mathbf{F}_4=\begin{bmatrix}0&\cdots&0&e^{\mathbf{A}_0T_f}\\0&0&0&0\\&\ddots&&\\&&0&\\0&&&0\end{bmatrix} \tag{17}$$

Therefore, under one tooth passing period, the transition matrix of the system $\boldsymbol{\Phi}$ is derived as:

$$\boldsymbol{\Phi}=(\mathbf{I}-\mathbf{D}_4-\frac{\tau}{720}\mathbf{E}_4)^{-1}(\mathbf{F}_4-\frac{\tau}{720}\mathbf{E}_4) \tag{18}$$

Finally, the prediction of the milling stability will be performed based on the Floquet theory.

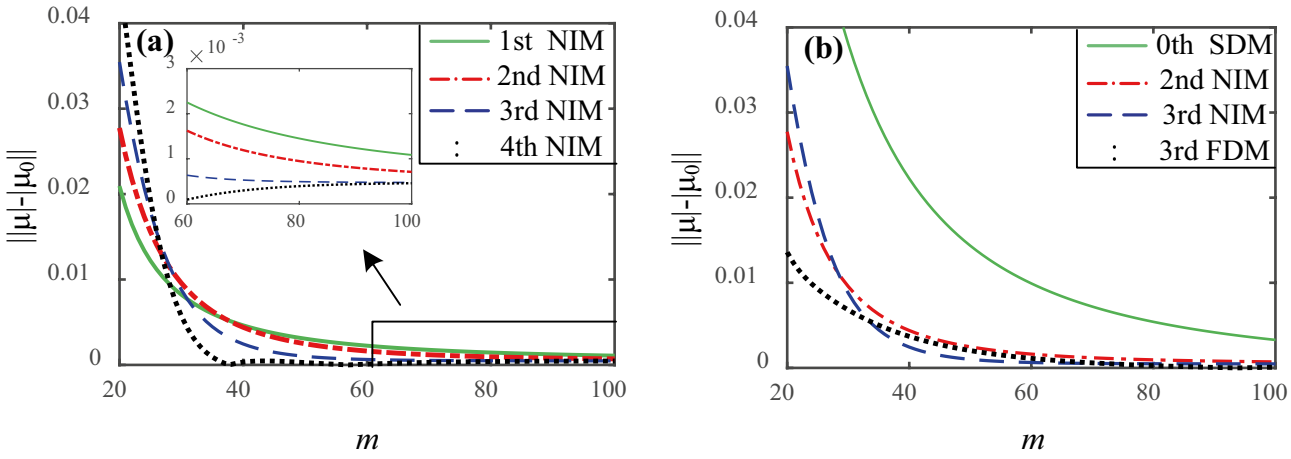

Fig. 2 Convergence rates from the NIMs (**a**) and the discretization methods (**b**) under $a_p = 0.2$ mm

3 The effect of the order of the NIFs on milling stability prediction

To easily distinguish the built NIMs with third order and fourth order, the two methods are named as 3rd NIM and 4th NIM, respectively. Similarly, the first two-order NIMs in reference [31] are described as 1st NIM and 2nd NIM, respectively. Then, the computational performance among the four methods is compared to analyze the effect of the polynomial order on the stability prediction. Meantime, the 0th SDM [10] and 3rd FDM [21] are introduced as a contrast. In reference [21], with the slightly loss of the computational efficiency, the 3rd FDM has higher computational accuracy compared with the existing FDMs.

The rate of convergence analysis for these NIMs is performed firstly. The local discretization error was usually used to verify the discretization performance [12]. The used system parameters of the single degree-of-freedom (DOF) milling dynamic model keep the same as these in reference [31]. The cutting parameters choose the spindle speed n of 5000 rpm, down milling, radial depth of cut ratio $a_e/D = 1$, and the axial cutting depths a_p of 0.2 mm, 0.5 mm, and 1 mm. Then, the convergence rates are obtained using the above methods respectively, and are illustrated in Figs. 2, 3 and 4. As shown in Figs. 2a, 3a and 4a, it can be clearly seen that the convergence rate becomes faster when the interpolation order increases among the first four order NIMs. In these sub-figures (b), the convergence rate of the 3rd NIM is faster than that of the 3rd FDM, whereas the 3rd FDM converges faster than 2nd NIM.

To verify the computational accuracy, the stability lobe diagrams (SLDs) of the milling system are predicted by the built NIMs and the discretization methods, respectively.

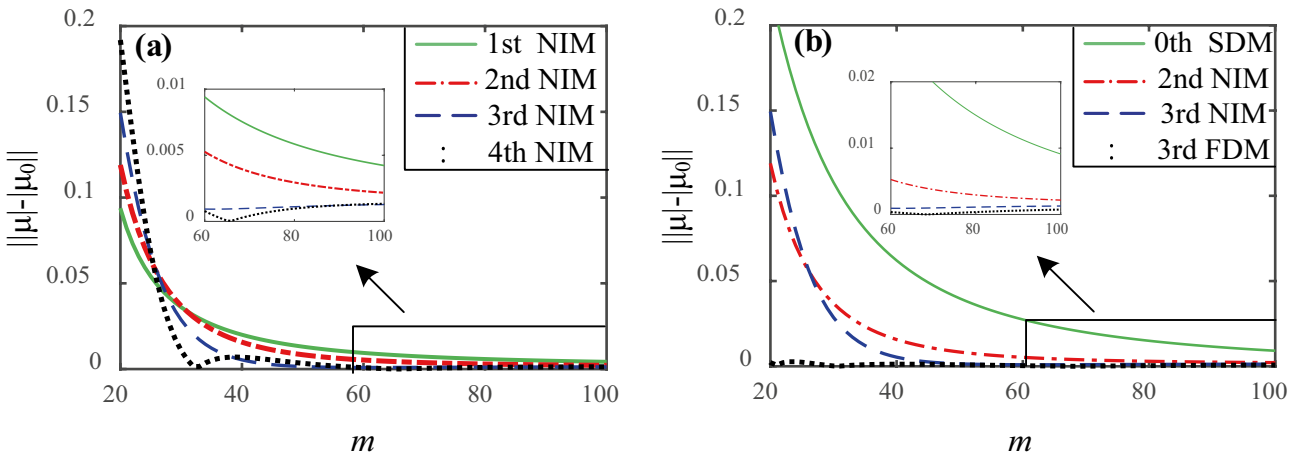

Fig. 3 Convergence rates from the NIMs (**a**) and the discretization methods (**b**) under $a_p = 0.5$ mm

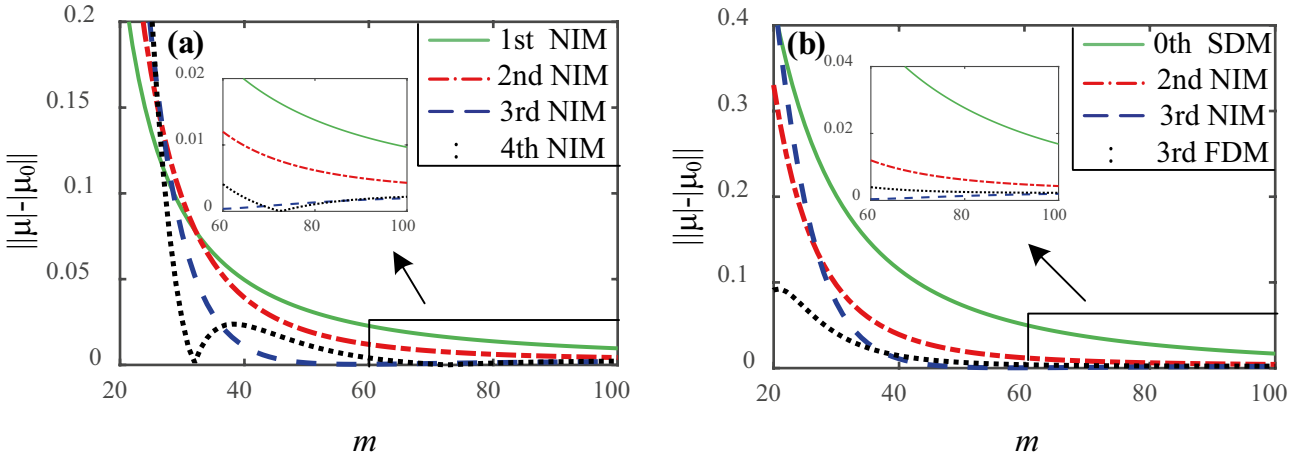

Fig. 4 Convergence rates from the NIMs (**a**) and the discretization methods (**b**) under $a_p = 1$ mm

The used system parameters remain unchanged. The cutting parameters are set, including 5000 rpm $< n <$ 10,000 rpm and $a_e/D = 1$. Under the different discretization number m, the obtained SLDs are shown in Figs. 5, 6 and 7.

In Figs. 5, 6 and 7, the accurate curves are obtained based on the 2nd FDM with $m = 200$ as the reference curves [14, 21]. In these sub-figures (a), the SLDs from the NIMs with higher order are more close to the reference curve, which demonstrate the corresponding NIMs have higher computational accuracy. From the sub-figures (b), the computational accuracy of the 3rd NIM is better than that of the 3rd FDM, but the 3rd FDM shows the higher accuracy than the 2nd NIM. The relevant computational cost is listed in Table 1, which is visually illustrated in Fig. 8. It can be clearly observed from the figure that the computational time of every predicted method lengthens when the discretization number increases. Under the same discretization number, the runtime from 0th SDM is the longest. For the NIMs, the computational time increases when the interpolation order increases. Therefore, the computational results reveal that the higher-order NIM has higher computational accuracy, but will lose the computational efficiency.

4 Improved numerical integration method and verification

Based on the Lagrange interpolation polynomial, the local discretization errors of the third-order and fourth-order NIMs are $O(\tau^5)$ and $O(\tau^6)$, respectively. The corresponding local discretization error in the NIMs [31] are $O(\tau^3)$ and $O(\tau^4)$, respectively. However, for these NIMs, the actual local discretization error is $O(\tau^3)$ due to the effect of the trapezoidal formula [23]. In order to decrease the local discretization error of the proposed NIMs, the Simpson rule as the accurate two-step method is introduced since its truncation error is $O(\tau^5)$.

In the first four order NIMs, the trapezoidal formula is used to describe the response points that cannot be expressed by the Lagrange polynomial, such as Eqs. (9) and (15). Thus, the Simpson rule is introduced to instead the trapezoidal formula in these NIMs. The third-order NIM is used as the example for the improvement demonstration using the Simpson rule. Equation (9) in 3rd NIM is rewritten as:

$$\mathbf{x}(t_i) = e^{\mathbf{A}_0(t_i - t_{i-1})}\mathbf{x}(t_{i-1}) + \frac{\tau}{12}\left\{\begin{array}{l} 4e^{\mathbf{A}_0(t_i - t_{i-2})}\mathbf{A}(t_{i-2})[\mathbf{x}(t_{i-2}) - \mathbf{x}(t_{i-2} - T)] + \\ 16e^{\mathbf{A}_0(t_i - t_{i-1})}\mathbf{A}(t_{i-1})[\mathbf{x}(t_{i-1}) - \mathbf{x}(t_{i-1} - T)] + \\ 4\mathbf{A}(t_i)[\mathbf{x}(t_i) - \mathbf{x}(t_i - T)] \end{array}\right\} \tag{19}$$

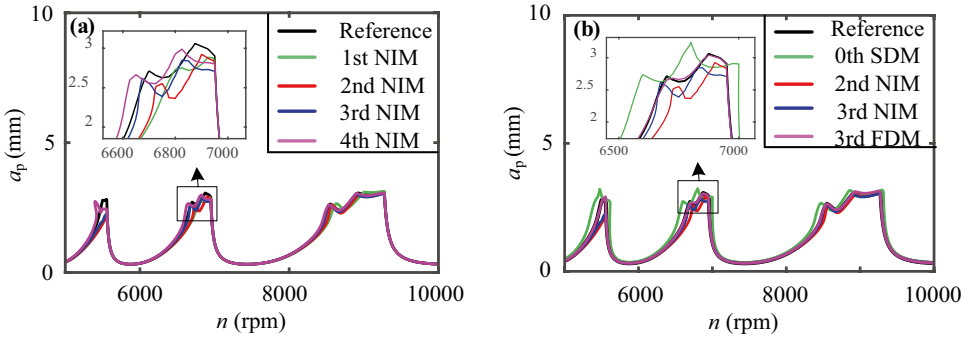

Fig. 5 The SLDs predicted by the NIMs (**a**) and the discretization methods (**b**) under $m = 40$

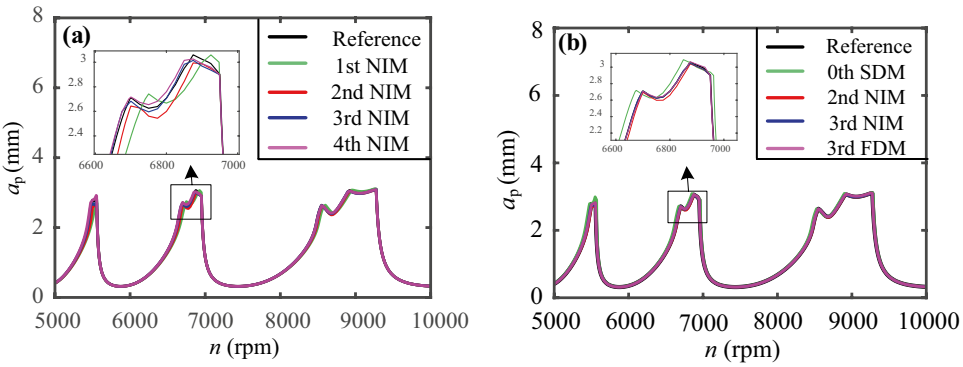

Fig. 6 The SLDs predicted by the NIMs (**a**) and the discretization methods (**b**) under $m = 60$

Similarly, the first two-order NIMs [31] are improved by the Simpson rule as well. The improved first three-order NIMs are renamed by 1st S-NIM, 2nd S-NIM, and 3rd S-NIM, respectively. Then, the convergence rate and the SLDs are investigated to verify the computational performance of the improved NIMs.

4.1 Analysis of the convergence rate

For the single DOF milling dynamic model, the rates of convergence analysis for the improved NIMs are performed. The used system parameter and cutting parameter are consistent with those in Sect. 3. Under the different axial cutting depths, the local discretization errors of the improved NIMs are shown in Figs. 9, 10 and 11. These sub-figures (a) clearly demonstrate that the convergence rates of 1st S-NIM and 2nd S-NIM are obviously increased compared with those of the corresponding former first two-order NIMs, and the 2nd S-NIM converges faster than the 3rd NIM. However, the 3rd S-NIM converges slower than the 3rd NIM. Meantime, the relative sub-figures (b) compare the convergence rates between the improved NIMs and the discretization methods. In Fig. 9b, when a_p is 0.2 mm, the 2nd S-NIM converges faster than the 3rd FDM. When a_p increases to 0.5 mm or 1 mm, the 2nd S-NIM converges slowly under the smaller value of the discretization number m. However, when m increases to some certain value, the convergence rate of the 2nd S-NIM is faster than that of the 3rd FDM, which can be illustrated in Figs. 10b and 11b.

Through the above analysis, it could be concluded that the NIMs with the trapezoidal formula converge faster and faster when the order of the used NIFs increases, as shown in Figs. 2, 3 and 4. When introducing the Simpson rule instead of the trapezoidal formula, the actual local discretization error of the improved NIMs decreases. The convergence rates of the improved NIMs with the first two orders are increased, but the higher-order improved NIM, such as the 3rd S-NIM, converges slower than the 3rd NIM, as shown in Figs. 9, 10 and 11. In other words, when one kind of the high-order NIF is used to estimate the system responses, the higher-order NIF can improve the prediction performance. When simultaneously introducing two kinds of the higher-order NIFs, such as the Lagrange integral formula and Simpson rule, the improved NIM may not has high prediction performance. This is due to the reason that the different higher-order NIFs together used to describe the system responses lead to the increase of the accumulative error, which deteriorates the computational performance [21]. Therefore, in order to achieve the milling stability prediction accurately and efficiently, the used different NIFs and their order should be optimized, such as 2nd S-NIM.

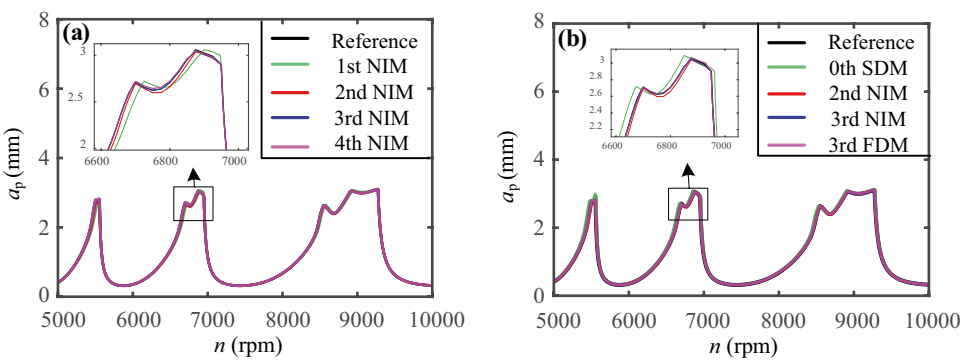

Fig. 7 The SLDs predicted by the NIMs (**a**) and the discretization methods (**b**) under $m = 80$

Table 1 Computational cost from the NIMs and the discretization methods (unit: s)

Methods	$m=40$	$m=60$	$m=80$
0th SDM	167.5	260.0	372.0
3rd FDM	47.1	83.4	136.6
4th NIM	32.3	64.6	99.4
3rd NIM	27.8	58.7	91.6
2nd NIM	24.2	50.7	76.6
1st NIM	21.8	43.0	64.9

4.2 Prediction of the stability lobe diagram

To further compare the computational performance of the 2nd S-NIM and 3rd FDM, the SLDs for the single-DOF and two-DOF milling dynamic models are predicted, respectively. Some machining parameters are set, which mainly include 5000 rpm $< n <$ 10,000 rpm and $a_e/D = 1$. Under the discretization number m with 40, 60, and 80, the calculated SLDs are illustrated in Fig. 12, and the corresponding time cost is listed in Table 2. The

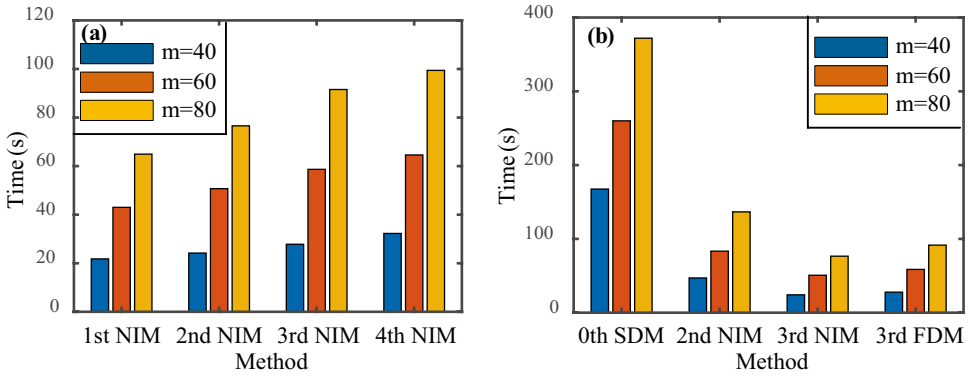

Fig. 8 Comparison of computational cost from the NIMs (**a**) and the discretization methods (**b**) under the different m

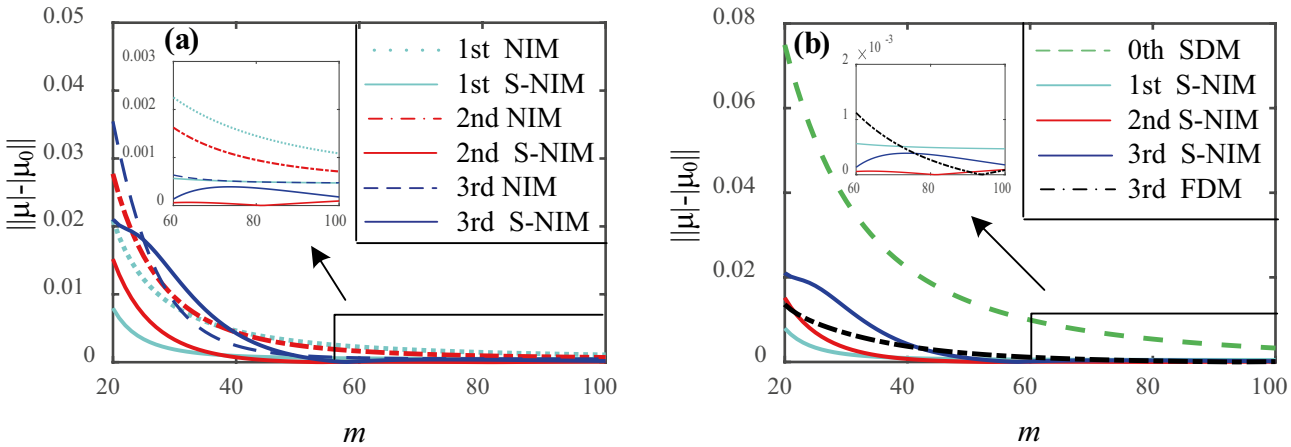

Fig. 9 Convergence rates from the improved NIMs (**a**) and the discretization methods (**b**) under $a_p = 0.2$ mm

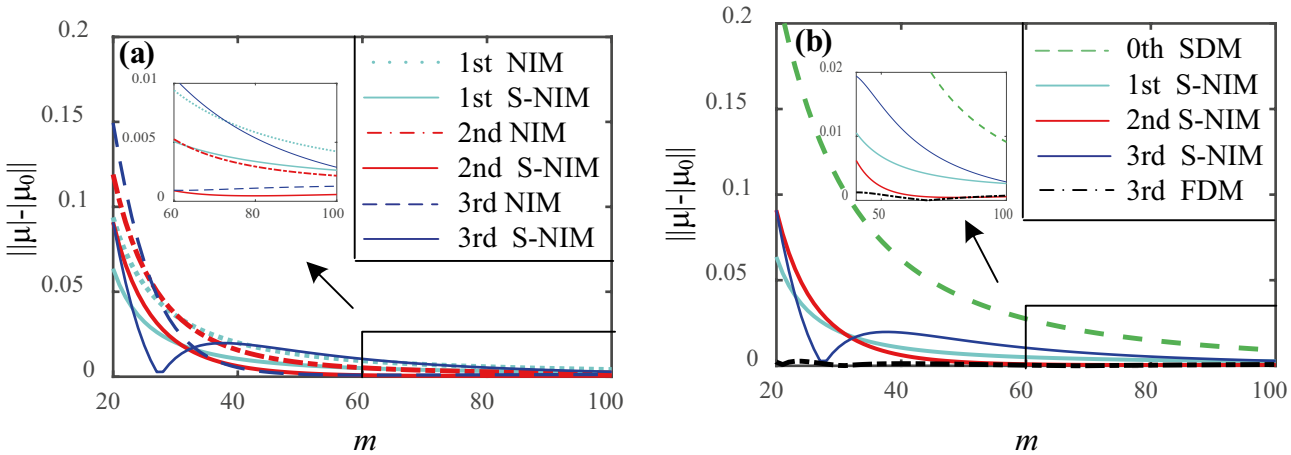

Fig. 10 Convergence rates from the improved NIMs (**a**) and the discretization methods (**b**) under $a_p = 0.5$ mm

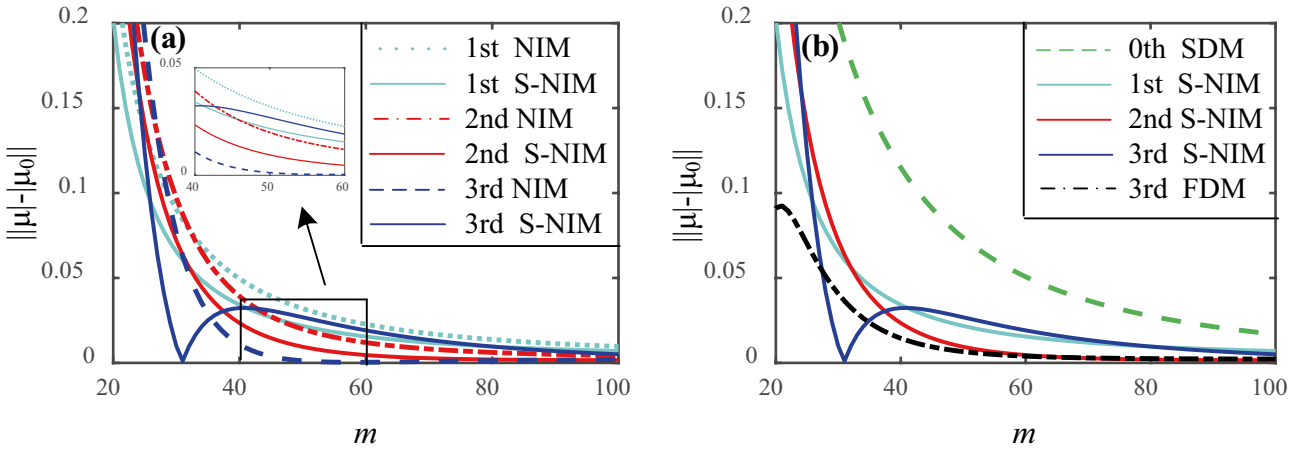

Fig. 11 Convergence rates from the improved NIMs (**a**) and the discretization methods (**b**) under $a_p = 1$ mm

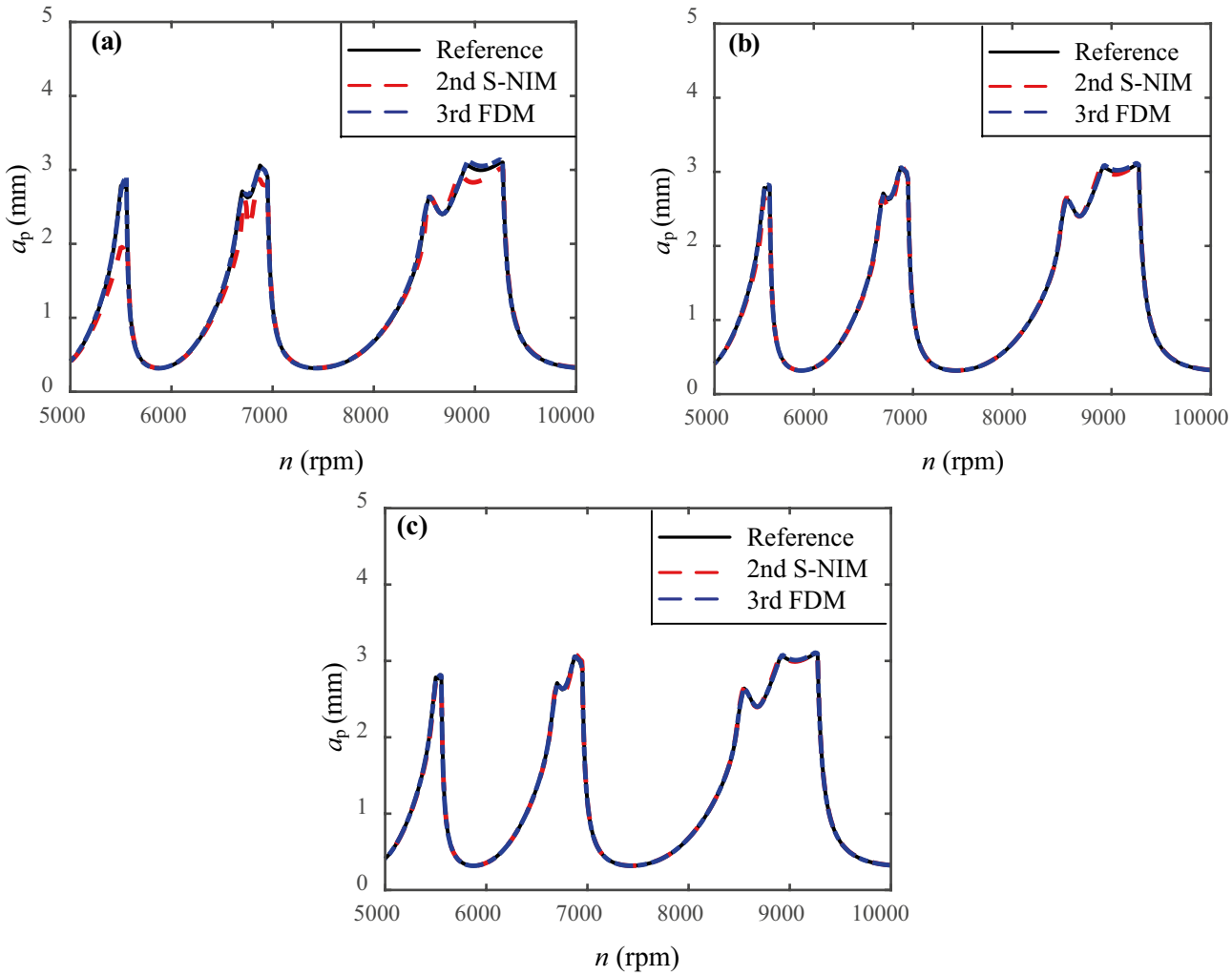

Fig. 12 The SLDs from the 2nd S-NIM and 3rd FDM under $m = 40$ (**a**), 60 (**b**), and 80 (**c**), respectively

Table 2 Computational cost from the 2nd S-NIM and 3rd FDM (Unit: s)

Methods	$m=40$	$m=60$	$m=80$
3rd FDM	47.1	83.4	136.6
2nd NIM	24.2	50.7	76.6
2nd S-NIM	25.5	52.8	78.6

Table 3 Computational cost from the 2nd S-NIM and 3rd FDM under $a_e/D=0.1$ and 0.05 (Unit: s)

Methods	$a_e/D=0.1$	$a_e/D=0.05$
3rd FDM	64.1	64.3
2nd S-NIM	39.8	36.7

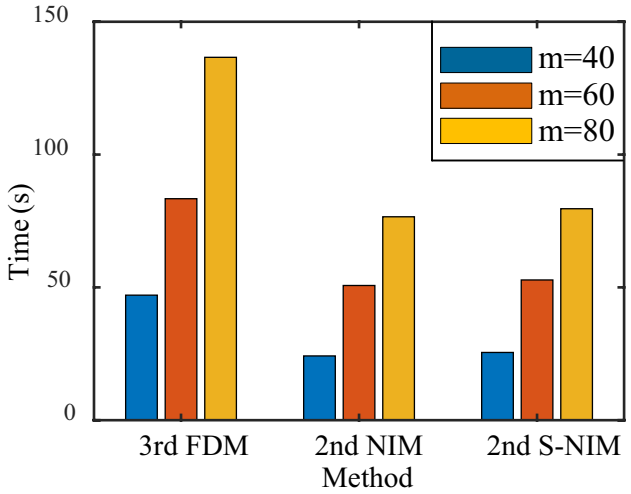

Fig. 13 Comparison for the computational cost from the 2nd S-NIM and 3rd FDM under the different m

figure clearly demonstrates that both of the SLDs from the 2nd S-NIM and 3rd FDM are close to the reference curve. As shown in Fig. 13, the computational time of the 2nd S-NIM is significantly less than that of the 3rd FDM, and it is almost equal to that of the 2nd NIM. The predicted results reveal that the 2nd S-NIM improves the computational accuracy, ensuring the computational efficiency.

For the two-DOF milling dynamic model, the system parameters are the same with those in single-DOF model. The discretization number m is set to 40, and the spindle speed is under the range of 5000 to 10,000 rpm. Under $a_e/D=0.1$ and 0.05, the SLDs are obtained by using the 2nd S-NIM and 3rd FDM respectively, as shown in Fig. 14. The relative computational time is listed in Table 3. When $a_e/D=0.1$, the SLDs from 2nd S-NIM and 3rd FDM are near to the reference curve. However, when $a_e/D=0.05$, the SLD curve from 3rd FDM is far away from the reference curve. Meantime, Table 3

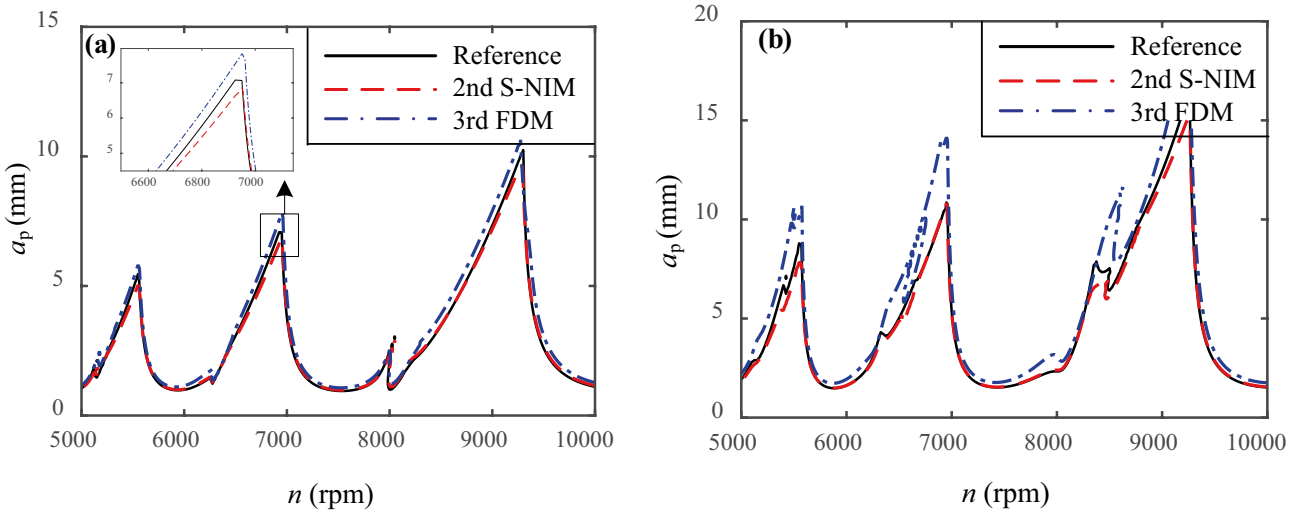

Fig. 14 The SLDs from the 2nd S-NIM and 3rd FDM under $a_e/D=0.1$ (**a**) and 0.05 (**b**)

demonstrates the higher computational efficiency of the 2nd S-NIM. Based on the above analysis, compared with the higher-order predicted method, such as 3rd FDM and 3rd NIM, the 2nd S-NIM shows the better computational performance.

5 Conclusions

In this paper, a numerical integration method (NIM) is improved based on the Lagrange-Simpson hybrid interpolation scheme. The main conclusions are summarized as follows:

1. According to the Lagrange interpolation scheme, the third-order and fourth-order numerical integration formulas (NIFs) are constructed to estimate the integral term of the integral equation described the milling dynamic process, respectively.
2. The higher-order NIMs are proposed based on the constructed NIFs, in which the tooth passing period is discretized equally. Then, the effect of the interpolation order of the NIFs on the chatter stability is analyzed by calculating the convergence rate and the SLDs. The results show that the computational accuracy is improved when the interpolation order of the NIFs increases, whereas the corresponding computational cost also increases. Meantime, the convergence rate of the 3rd NIM is faster than that of the 3rd FDM, whereas the 3rd FDM converges faster than 2nd NIM.
3. In order to increase the computational accuracy, the Simpson scheme is used to improve the NIMs. The convergence rate and the SLDs are investigated by using the improved NIMs and the existing discretization methods, respectively. When introducing the Simpson scheme, the local discretization error of the NIM can be decreased, whereas the corresponding computational performance may not necessarily increase. The different NIFs and the relative order should be optimized, where the optimized 2nd S-NIM shows the better computational performance compared with the 3rd FDM and 3rd NIM.

Appendix. Matrix $\mathbf{E}_4$

$$\mathbf{E}_4=\begin{bmatrix} 0 & & & & & & & \\ 251e^{\mathbf{A}_0\tau}\mathbf{A}_1 & 646\mathbf{A}_2 & -264e^{-\mathbf{A}_0\tau}\mathbf{A}_3 & 106e^{-2\mathbf{A}_0\tau}\mathbf{A}_4 & -19e^{-3\mathbf{A}_0\tau}\mathbf{A}_4 & & & \\ & \ddots & \ddots & \ddots & \ddots & & & \\ & & 251e^{\mathbf{A}_0\tau}\mathbf{A}_{m-3} & 646\mathbf{A}_{m-2} & -264e^{-\mathbf{A}_0\tau}\mathbf{A}_{\mathrm{m-1}} & 106e^{-2\mathbf{A}_0\tau}\mathbf{A}_m & -19e^{-3\mathbf{A}_0\tau}\mathbf{A}_{m+1} & \\ & & & 360e^{\mathbf{A}_0\tau}\mathbf{A}_{m-2} & 360\mathbf{A}_{m-1} & & & \\ & & & & 360e^{\mathbf{A}_0\tau}\mathbf{A}_{m-1} & 360\mathbf{A}_m & & \\ & & & & & 360e^{\mathbf{A}_0\tau}\mathbf{A}_m & 360\mathbf{A}_{m+1} & \end{bmatrix}$$

Author contribution Yan Xia, Yi Wan, Guosheng Su, and Chonghai Xu contributed to the conceptualization and methodology; Yan Xia, Jin Du, and Peirong Zhang performed the investigation and analysis; Yan Xia wrote the manuscript.

Funding This paper was funded by National Natural Science Foundation of China (Grant No. 51975336) and Key Research and Development Program of Shandong Province (Grant No. 2019JZZY010112, 2020JMRH0202).

Declarations

Conflict of interest The authors declare no competing interests.

References

1. Quintana G, Ciurana J (2011) Chatter in machining processes: a review. Int J Mach Tools Manuf 51(5):363–376
2. Yue CX, Gao HN, Liu XL, Liang SY, Wang LH (2019) A review of chatter vibration research in milling. Chin J Aeronaut 32(2):215–242
3. Ding Y, Zhu LM, Zhang XJ, Ding H (2010) A full-discretization method for prediction of milling stability. Int J Mach Tools Manuf 50(5):502–509
4. Altintaş Y, Budak E (1995) Analytical prediction of stability lobes in milling. CIRP Ann-Manuf Technol 44(1):357–362
5. Budak E, Altintas Y (1998) Analytical prediction of chatter stability in milling—part I: general formulation. J Dyn Syst Meas Control 120(1):22–30
6. Merdol SD, Altintas Y (2004) Multi frequency solution of chatter stability for low immersion milling. J Manuf Sci Eng 126(3):459–466
7. Altıntas Y, Engin S, Budak E (1999) Analytical stability prediction and design of variable pitch cutters. J Manuf Sci Eng 121(2):173–178
8. Turner S, Merdol D, Altintas Y, Ridgway K (2007) Modelling of the stability of variable helix end mills. Int J Mach Tools Manuf 47(9):1410–1416
9. Li WT, Wang LP, Yu G (2020) An accurate and fast milling stability prediction approach based on the Newton-Cotes rules. Int J Mech Sci 177:105469
10. Insperger T, Stépán G (2004) Updated semi-discretization method for periodic delay-differential equations with discrete delay. Int J Numer Methods Eng 61:117–141
11. Insperger T, Stépán G, Turi J (2008) On the higher-order semi-discretizations for periodic delayed systems. J Sound Vib 313(1):334–341
12. Insperger T (2010) Full-discretization and semi-discretization for milling stability prediction: Some comments. Int J Mach Tools Manuf 50(7):658–662

13. Zhan DN, Jiang SL, Niu JB (2020) Sun YW (2020) Dynamics modeling and stability analysis of five-axis ball-end milling system with variable pitch tools. Int J Mech Sci 182:105774
14. Ding Y, Zhu LM, Zhang XJ, Ding H (2010) Second-order full-discretization method for milling stability prediction. Int J Mach Tools Manuf 50(10):926–932
15. Tang XW, Peng FY, Yan R, Gong YH, Li YT, Jiang LL (2017) Accurate and efficient prediction of milling stability with updated full-discretization method. Int J Adv Manuf Technol 88(9):2357–2368
16. Guo Q, Sun YW, Jiang Y (2012) On the accurate calculation of milling stability limits using third-order full-discretization method. Int J Mach Tools Manuf 62:61–66
17. Liu YL, Zhang DH, Wu BH (2012) An efficient full-discretization method for prediction of milling stability. Int J Mach Tools Manuf 63:44–48
18. Huang C, Yang WA, Cai XL, Liu WC, You YP (2020) An efficient third-order full-discretization method for prediction of regenerative chatter stability in milling. Shock Vib 2020:9071451
19. Wu Y, You YP, Jiang JJ (2020) New predictor-corrector methods based on piecewise polynomial interpolation for milling stability prediction. Mach Sci Technol 24(5):688–718
20. Zhang Y, Liu KN, Zhao WY, Zhang W, Dai F (2020) Stability analysis for milling process with variable pitch and variable helix tools by high-order full-discretization methods. Math Probl Eng 2020:4517969
21. Xia Y, Wan Y, Luo XC, Liu ZQ, Song QH (2021) Milling stability prediction based on the hybrid interpolation scheme of the Newton and Lagrange polynomials. Int J Adv Manuf Technol 112(5–6):1501–1512
22. Ding Y, Zhu LM, Zhang XJ, Ding H (2011) Numerical integration method for prediction of milling stability. J Manuf Sci Eng-Trans ASME 133(3):1–9
23. Zhang Z, Li HG, Meng G, Liu C (2015) A novel approach for the prediction of the milling stability based on the Simpson method. Int J Mach Tools Manuf 99:43–47
24. Ozoegwu CG (2016) High order vector numerical integration schemes applied in state space milling stability analysis. Appl Math Comput 273:1025–1040
25. Tao JF, Qin CJ, Liu CL (2017) Milling stability prediction with multiple delays via the extended Adams-Moulton-Based method. Math Probl Eng 2017:7898369
26. Zhi HY, Yan XG, Du J, Cao QC, Zhang TS (2018) Prediction of the milling stability based on the implicit Adams method. J Mech Eng 54(23):223–232
27. Dun YC, Zhu LD, Wang SH (2020) Multi-modal method for chatter stability prediction and control in milling of thin-walled workpiece. Appl Math 80:602–624
28. Butcher EA, Bobrenkov OA, Bueler E, Nindujarla P (2009) Analysis of milling stability by the Chebyshev collocation method: algorithm and optimal stable immersion levels. J Comput Nonlinear Dyn 4(3):31003
29. Li H, Han P, Zhang LL (2016) Milling stability analysis based on Chebyshev segmentation. J Northeast Univ 37(4):538–542
30. Qin CJ, Tao JF, Shi HT, Xiao DY, Li BC, Liu CL (2020) A novel Chebyshev-wavelet-based approach for accurate and fast prediction of milling stability. Precis Eng 62:244–255
31. Xia Y, Wan Y, Luo XC, Liu ZQ, Song QH (2021) An improved numerical integration method to predict the milling stability based on the Lagrange interpolation scheme. Int J Adv Manuf Technol 116:2111–2123